Exp Fluids (2015) 56:138
DOI 10.1007/s00348-015-2000-0

RESEARCH ARTICLE

Nanoscale sensing devices for turbulence measurements

Y. Fan[1] · G. Arwatz[1] · T. W. Van Buren[1] · D. E. Hoffman[1] · M. Hultmark[1]

Received: 9 February 2015 / Revised: 28 April 2015 / Accepted: 21 May 2015 / Published online: 20 June 2015

Abstract A collection of nanoscale sensing devices developed specifically for high-frequency turbulence measurements is presented. The new sensors are all derived from the nanoscale thermal anemometry probe (NSTAP), which uses a free-standing platinum wire as active sensing element. Each sensor is designed and fabricated to measure a specific quantity and can be customized for special applications. In addition to the original NSTAP (for single-component velocity measurement), the new sensors include the T-NSTAP (for temperature measurement), the x-NSTAP (for two-component velocity measurement), and the q-NSTAP (for humidity measurement). This article provides a summary of the NSTAP family including details of design and fabrication as well as presentation of flow measurements using these sensors. Also, a custom-made constant-temperature anemometer that allows proper operation of the NSTAP sensors will be introduced.

1 Introduction

Turbulent flow parameters, such as the velocity and temperature, vary significantly and irregularly in both space and time. To attain a fundamental understanding of turbulence, it is crucial to accurately capture and characterize these fluctuating quantities. Hot-wire anemometry (HWA), despite having many limitations (intrusive, point measurements, typically limited to one or two components), is still the preferred tool for obtaining high Reynolds number turbulent flow measurements, mainly due to its relatively high temporal and spatial resolution and continuous signals. Results obtained by HWA can be used to construct and examine the frequency content of turbulence, as well as provide information on correlations and other statistics (see, e.g., Wyngaard 1968; Nickels et al. 2007; Bodenschatz et al. 2014; Smits and Hultmark 2014).

When measuring the fluctuating quantities in turbulence with hot- and cold-wire probes, it is important to ensure that the probes have sufficient spatial and temporal resolution to resolve both the smallest scales and highest frequencies contained in the flow. Otherwise, vital information will be filtered and the results will be biased. Higher Reynolds numbers imply that the ratio of the largest to the smallest scales increases, and thus for a fixed-size facility, the smallest scales decrease in size. One way to overcome this issue is to increase the smallest scales within the flow by increasing the size of the facility itself. Examples of this approach can be found in the F1 wind tunnel at ONERA in France or the Long Pipe at CICLoPE in Italy (Brocard and Desplas 1984; Talamelli et al. 2009). Although effective, this requires a large commitment of finances and manpower. Conversely, the sensor size can be made smaller so that it can better resolve the smallest flow scales, which is the primary focus of this article.

For a hot or cold wire, a smaller sensor implies a shorter wire, which will have better spatial resolution, while the smaller thermal mass improves the frequency response. However, simply reducing the length of the wire does not always yield more accurate results since end-conduction effects are introduced if the wire length to diameter ratio (ℓ/d) is too small. These effects become significant when the heat transfer through the ends of the wire filament to the wire support is

This article belongs to a Topical Collection of articles entitled Extreme Flow Workshop 2014. Guest editors: I. Marusic and B. J. McKeon.

✉ Y. Fan
yf@princeton.edu

[1] Department of Mechanical and Aerospace Engineering, Princeton University, Princeton, NJ, USA

a non-negligible part of the total heat transfer (Willmarth and Sharma 1984). The commonly accepted required aspect ratio, ℓ/d, for hot wires is at least 200 (Ligrani and Bradshaw 1987) and 1000 for cold wires (CW) (Smits et al. 1978).

With the rapid development of micromachining and integrated circuit technology, possibilities of making smaller sensors became viable using the microelectromechanical system (MEMS) approach. Löfdahl et al. (1989) and Löfdahl et al. (1992) built an anemometer on a small integrated device using MEMS techniques with chips that can measure single- or dual-component velocity. Measurements acquired using these sensors compared well to conventional hot wires; however, the sensing chips only slightly improved the spatial resolution of the conventional wires due to their relatively large dimensions. Chen et al. (2003) developed a process to fabricate multicomponent hot-wire sensors with a much smaller size (as small as 50 μm × 6 μm × 2.7 μm) on different substrates. Unfortunately, the geometry of the sensor made it unsuitable for conventional turbulence measurements and end-conduction became an important limitation. Kim et al. (2004) built a circular type of flow sensor with heated strips that can determine both flow direction and speed without reorienting the sensor, but this sensor was not suitable for investigating turbulence since the substrate on which the sensors are planted will obstruct and therefore alter the flow field. Attempts to fabricate MEMS flow sensors with polysilicon were also made, but those either did not improve the resolution much (Ebefors et al. 1998) or suffered from end-conduction effects because of low aspect ratio (Jiang et al. 1994; Tai et al. 1993; Ho et al. 1993). Wang et al. (2007) took a different approach by fabricating a microcantilever structure for flow measurement, but the resolution was worse than conventional hot-wire sensors.

The necessity for smaller measurement probes motivated the design and fabrication of accurate nanoscale-sized probes specifically designed for turbulence measurements. The nanoscale thermal anemometer probe (NSTAP) was first proposed by Kunkel et al. (2006). These miniature hot wires have been shown to significantly improve high Reynolds number velocity measurements (Bailey et al. 2010; Vallikivi et al. 2011), as well as high-frequency temperature measurements (Arwatz et al. 2015). In this article, the various NSTAP probe types will be explored, detailing unique fabrication techniques as well as presenting flow measurements corroborating their success.

2 Collection of NSTAP-derived sensors

2.1 Single-component velocity: NSTAP

Ligrani and Bradshaw (1987) suggested two criteria for accurate velocity measurements using hot wires in wall-bounded turbulence : $\ell/d \geq 200$ in order to reduce end-conduction effects and $\ell^+ = \ell u_\tau/\nu \leq 20$ to reduce spatial filtering. Here, ℓ is the length of the wire, ν is the fluid kinematic viscosity, and u_τ is the friction velocity. u_τ is defined as $u_\tau = \sqrt{\tau_w/\rho}$, where τ_w is the wall shear stress and ρ is the fluid density. Unfortunately, it is challenging to satisfy both criteria with conventional manufacturing methods; the typical hot-wire diameter is 2.5 or 5 μm; so according to the first criterion, the wire length needs to be at least 0.5 or 1 mm, respectively. However, in most high Reynolds number facilities, such spatial resolution is insufficient resulting in ℓ^+ values much >20. For example, in the High Reynolds Number Boundary Layer Wind Tunnel at Melbourne University (Hutchins et al. 2009), at $Re_\tau = 19{,}000$, wire lengths of $\ell < 350$ μm are required, and in the Princeton Superpipe (Zagarola and Smits 1998) at $Re_\tau = 100{,}000$, the wire length needs to be shorter than 13 μm to satisfy $\ell^+ \leq 20$.

The NSTAP was created as an effort to make significantly smaller hot-wire sensors for high Reynolds number turbulent velocity measurements, without significant spatial filtering or end-conduction effects. The NSTAP was developed by a team of researchers at Princeton University led by Professor Alexander Smits. The manufacturing and design approach was first presented by Kunkel et al. (2006). After several design and manufacturing iterations, Bailey et al. (2010) presented the first successful free-standing NSTAP, with a sensing element consisting of a platinum (Pt) filament measuring 60 μm × 2 μm × 100 nm. This sensor was machined using a pulsed UV laser, with less than ideal repeatability and fairly long manufacturing time. Subsequently, Vallikivi et al. (2011) substantially improved the manufacturing processes. The new sensor was manufactured by 3D-shaping the probes using a technique based on deep reactive ion etching (DRIE) and RIE lag, which replaced the unreliable laser step. The new process had significantly higher yield rate and resulted in more robust and less bulky sensor (Vallikivi and Smits 2014). Images and schematics comparing the two probes can be seen in Fig. 1. This research laid the framework for the design and fabrication processes used for all of the sensors presented in this paper.

As opposed to conventional probes, the cross section of an NSTAP is rectangular rather than circular, due to the method adopted to deposit the platinum wire. Therefore, the ℓ/d criterion for characterizing the end-conduction effects requires some modification. One approach is to consider the heat conducted to the wire supports versus the heat convected to the surrounding fluid. In an ideal hot wire, all the heat transfer is due to convection and not conduction. This approach was taken by Hultmark et al. (2011), which resulted in a new parameter for end-conduction effects, $\Gamma = (l/d)\sqrt{4a(\kappa_f/\kappa_w)Nu}$. This not only takes into

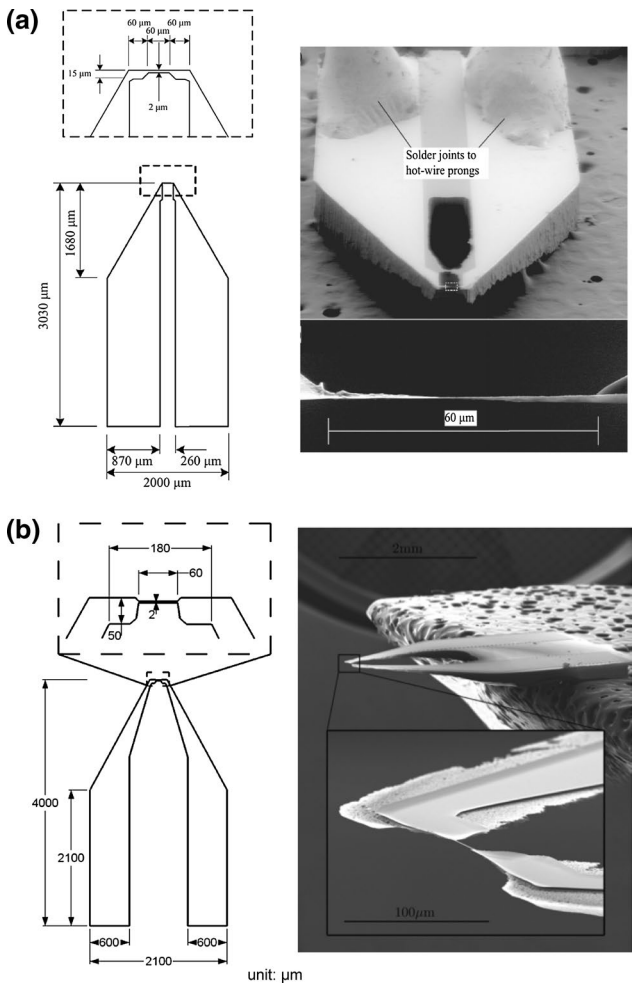

Fig. 1 Evolution of the NSTAP: **a** design and SEM image of the NSTAP by Bailey et al. (2010). **b** Design and SEM image of the improved NSTAP by Vallikivi et al. (2011)

consideration the geometry of the wire, but also allows for variations of the material properties (the thermal conductivity of the fluid κ_f, and of the wire κ_w) as well as Reynolds number effects (through Nusselt number, Nu). If one further refines this approach for a wire of any cross-sectional shape $\Gamma = \sqrt{a(\kappa_f/\kappa_w)Nu(A_s l/A_c l_c)}$, where l_c is the characteristic length of which the Nusselt number is defined; A_s and A_c correspond to the surface and cross-sectional area of the wire, respectively. The study further suggested that $\Gamma > 14$ to eliminate end-conduction effects. Although it is highly likely that this critical value depends on the geometry and dimensions of the wire, since the affected frequencies will change. The detailed effects of end-conduction on the frequency response remain to be investigated.

The regular NSTAP has been successfully operated with the Dantec Dynamics Streamline CTA system using the 1:1 bridge with external resistor. Detailed studies by Bailey et al. (2010) and Vallikivi et al. (2011) compared the

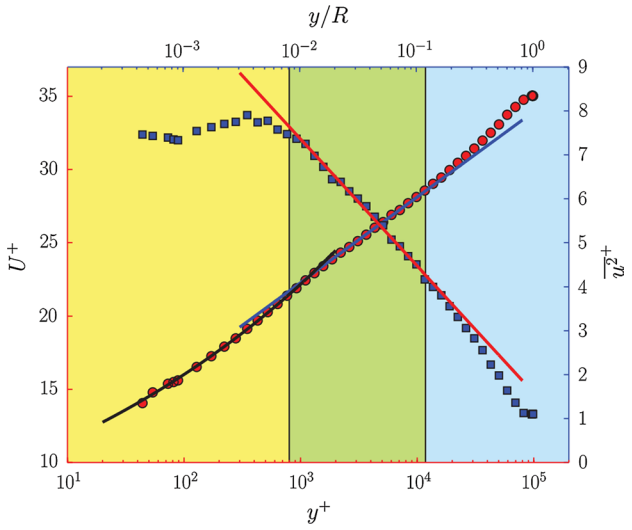

Fig. 2 Comparison of the non-dimensionalized mean streamwise velocity $U^+ = \overline{u}/u_\tau$ and the turbulence streamwise fluctuation profiles $\overline{u^2}^+ = u^2/u_\tau^2$ in the Superpipe at $Re_\tau = 98 \times 10^3$. *Red circles* are mean velocities, and *blue squares* are the turbulence fluctuations. *Blue* and *red lines* are the log laws for mean flow and turbulence fluctuations, respectively. Here, $y^+ = yu_\tau/\nu$. Figure excerpted from Hultmark et al. (2012)

NSTAP to conventional hot-wire probes. They found excellent agreement in the mean flow results and showed that the NSTAP has considerably higher spatial resolution and frequency response up to about 150 kHz in still air and even higher in flow using a square-wave test (it should be noted that according to Hutchins et al. 2015, the "true" frequency response is much lower than previously believed using a square-wave test. However, the NSTAP was shown to have a much higher "true" frequency response than conventional hot wire). The combination of the NSTAP and the Princeton Superpipe revealed an extensive logarithmic profile in the streamwise turbulence intensities at high Reynolds numbers. This was predicted more than 30 years earlier by Townsend (1976), but it had not been observed in experimental data due to a lack of well-resolved data at sufficiently high Reynolds numbers. The observed logarithmic region coincided with that in the mean velocity profile which can clearly be seen in Fig. 2, showing data at $Re_\tau = 98 \times 10^3$. The superior resolution of the NSTAP was clearly showed by Hutchins et al. (2015) who compared the frequency spectra measured by different hot-wire sensors at the same Reynolds number. The frequency content was shifted by altering the velocity and the pressure together. The single-wire NSTAP has also been used in other high Reynolds number facilities improving the accuracy of high Reynolds number data with reduced spatial and temporal filtering (Smits et al. 2011; Ashok et al. 2012; Marusic et al. 2013; Rosenberg et al. 2013; Hultmark et al. 2013; Bodenschatz et al. 2014; Sinhuber et al. 2015) (see Fig. 3a, b).

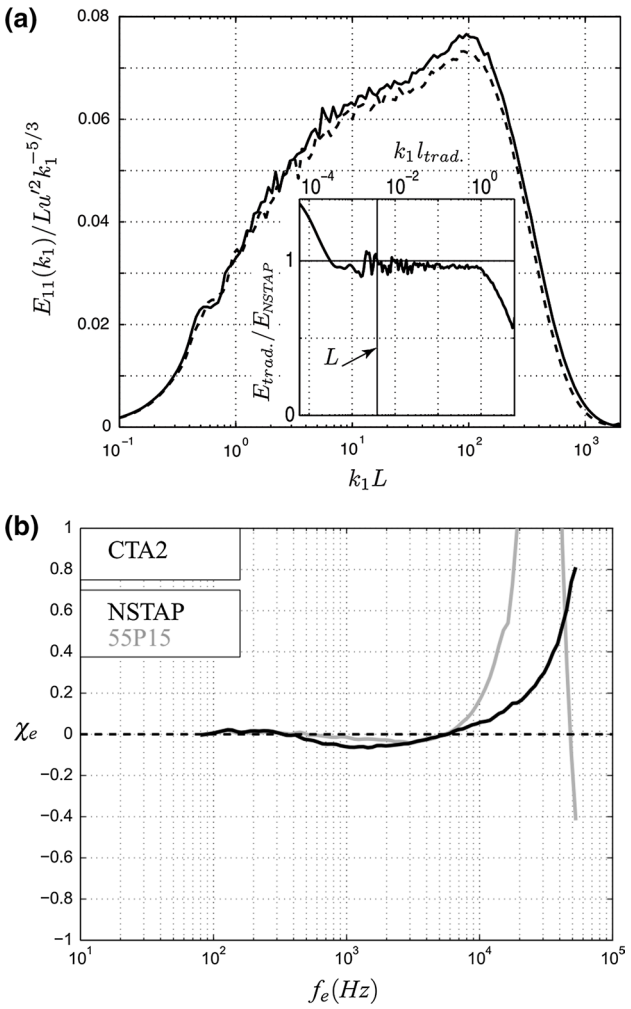

Fig. 3 **a** Comparison of a premultiplied spectrum acquired in the Göttingen Turbulence Facility with an NSTAP (*solid line*) and a conventional hot wire (*dashed line*), both with the Dantec CTA system at the Taylor Reynolds number $Re_\lambda = 730$. Here, E_{11} is the one-dimensional spectrum, k_1 is the streamwise wave number, and L is the integral length scale. It is clear that the NSTAP has less spatial filtering especially at smaller scales (captures more energy at larger wave numbers). Figure excerpted from Bodenschatz et al. (2014). **b** Comparison of the transfer function χ_e (ratio of premultiplied spectra at same Reynolds number but different time constants) for NSTAP (*black*) and conventional hot wire (*gray*), with the same anemometer. NSTAP is shown to be flat for a larger range of frequencies. Figure excerpted from Hutchins et al. (2015)

Five years after the first successful turbulence measurements with the NSTAP, it is now well established as a proven hot-wire probe, capable of small-scale turbulence measurements with both spatial and temporal resolution approximately one order of magnitude better than conventional hot-wire probes. It laid the ground work for other MEMS flow sensors such as Borisenkov et al. (2015) and the ones described in the following sections.

2.2 Two-component velocity: x-NSTAP

Despite the improved performance over conventional hot-wire probes, the regular NSTAP is limited to measuring a single component of velocity. However, in many flow configurations more than one component of velocity is of interest. For example, when studying wall-bounded flows, the wall-normal component of the fluctuating velocity, v, is of great significance and an important component in the governing equations. To measure the streamwise and wall-normal components, crossed hot-wire (or cross-wire) probes are commonly used. Cross-wires consist of two hot wires arranged in an "X" configuration. When placed in flow, each wire will register a combination of signals from both $\widetilde{u}$ and $\widetilde{v}$, the instantaneous velocities. Properly calibrated, each flow velocity component can be identified and reconstructed to obtain the magnitude and the direction of the instantaneous velocity in the plane of the wires. Furthermore, the cross-wire configuration allows one to obtain the covariance between the two velocity components, which is the Reynolds shear stress $\overline{uv}$.

Despite its importance to wall-bounded turbulence, there is currently a lack of high Reynolds number data of two-component turbulence measurements. For example, prior to 2007, the highest Reynolds number reported with more than one component of velocity was only about $Re_D \approx 5 \times 10^5$ by Laufer (1954) and Townes et al. (1972). Zhao and Smits (2007) used conventional cross-wire probes in the Princeton Superpipe and reported two-component measurements up to $Re_D = 9.8 \times 10^6$ (by pressurizing the working fluid). However, at that Reynolds number ℓ^+ exceeded 1200 (versus the suggested spatial filtering criterion $\ell^+ \leq 20$). Such poor spatial resolution unquestionably results in severe spatial filtering. A few attempts on creating MEMS cross-wire sensors have been made to address the issue of spatial filtering (such as Löfdahl et al. 1992; Chen et al. 2003), but those attempts either did not improve the spatial resolution or suffered from end-conduction effects.

Based on the newly designed NSTAP with a single inclined sensing element (Vallikivi et al. 2012), a MEMS cross-wire has been fabricated. The x-NSTAP is composed of two modified NSTAP probes with an inclined sensing wire of 60 μm × 2 μm × 100 nm at 45° angle, shown in Fig. 4a, b. The two probes form a cross with two sensing wires perpendicular to each other. The two modified probes are separated by an ultra-smooth DuPont Kapton film of 50 μm thickness that was patterned with gold traces [200 nm of gold (Au) with 10 nm of titanium (Ti) underneath as the adhesive layer] for electrical connection using photolithography. The gold traces are patterned on both sides of the Kapton film such that each probe has non-interfering electrical connections to the operating circuits. Conductive silver epoxy is used to attach the probes to the

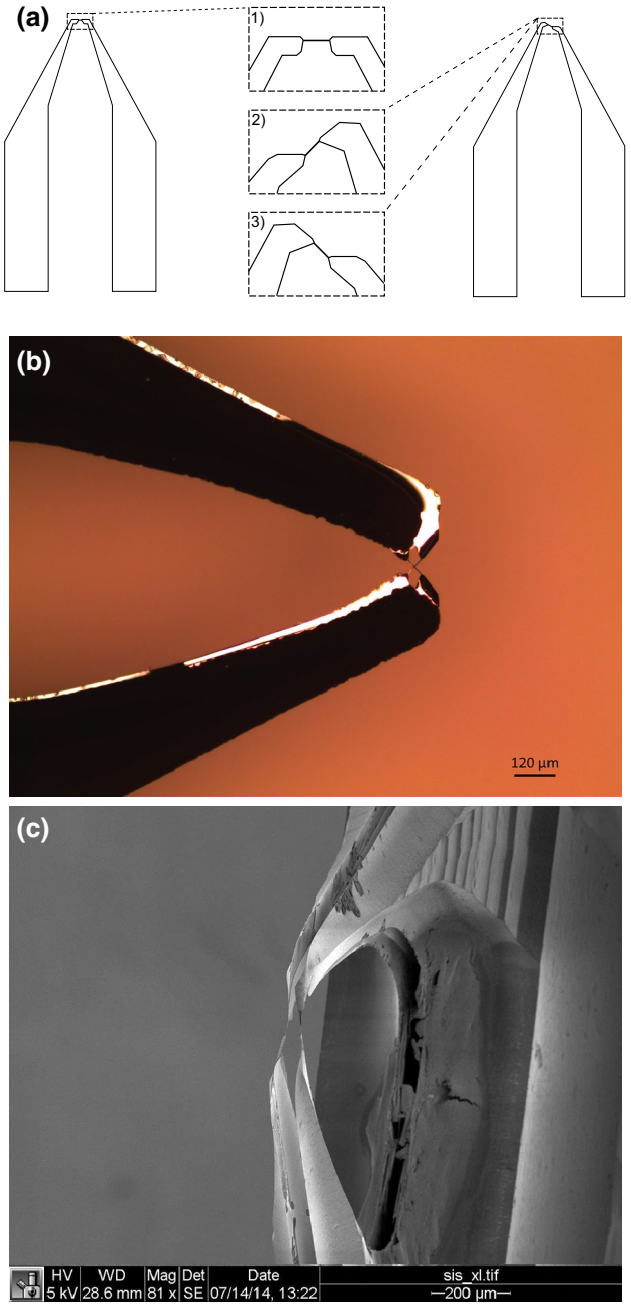

Fig. 4 **a** *Left* sketch of a regular NSTAP and its sensing element shown in 1). *Right* the modified NSTAP that has an inclined sensing wire at 45° angle from the streamwise direction, as shown in 2) and 3). **b** Microscope image of a recently developed nanoscale crossed hot wire (x-NSTAP), showing two-wire sensing elements are perpendicular to each other. **c** SEM image of the details of the two crossing platinum sensing elements

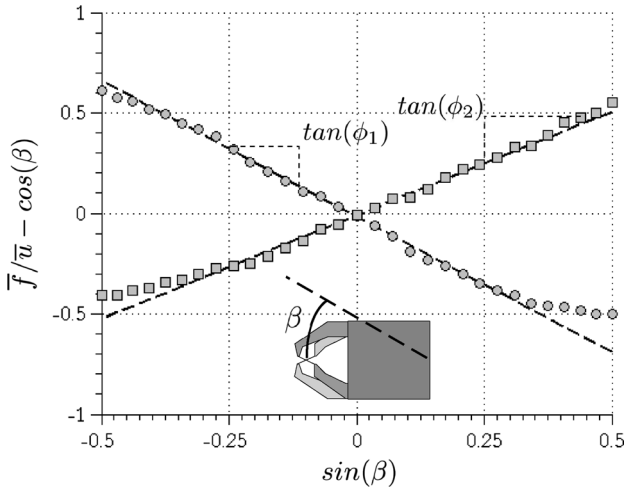

Fig. 5 x-NSTAP angle calibration. *Circle* and *square symbols* represent experimental results from each wire, and *lines* represent a linear fit with slope $\tan(\phi_i)$. Free stream velocity is $\overline{u} = 19$ m/s

Kapton film and cured under 15 N forces at 150 °C. The resulting x-NSTAP has a sensing volume of approximately 50 µm × 50 µm × 50 µm, more than one order of magnitude smaller in every direction compared to the conventional cross-wire sensors (Fig. 4c). In addition, the small thermal mass greatly improves the temporal resolution to that of a regular NSTAP.

Initial experiments were conducted to test the feasibility of these new miniature crossed hot-wire probes. An open loop wind tunnel capable of 5–20 m/s free stream velocities was utilized to generate a uniform flow field. The x-NSTAP probe was attached to custom-made ceramic probes with brass prongs and mounted on a manual rotary traverse to change the probe angle with respect to the flow field. The x-NSTAP wires were operated with a custom hot-wire anemometer described in Sect. 3. The wires were calibrated by fitting a fourth-order polynomial to nine voltage measurements over the velocity range of the wind tunnel (Fig. 14).

To find the wire cooling angles, the procedure proposed by Bradshaw (1971) was used, where measurements are made at various probe angles at a constant velocity. This assumption states that the hot-wire velocity ($\overline{f}$) when normalized by the measured mean streamwise velocity ($\overline{u}$, measured by a pitot probe) takes the form:

$$\frac{\overline{f}}{\overline{u}} = sin(\beta)tan(\phi) + cos(\beta), \quad (1)$$

where β is the probe yaw angle and ϕ is the cooling angle. Figure 5 presents an angle calibration of an x-NSTAP operated by the Princeton University Constant-Temperature Anemometer (PUCTA) (see Sect. 3). Here, we observe a linear relation and thus a constant cooling angle ϕ for yaw angles from −15° to 15°. Past those angles, the impact of the probe supports becomes clear, where the behavior deviates from linearity. From the slopes of the linear fit, the cooling angles are found to be 51° and 45° for the two wires, similar to the physical angles of the sensing element as seen in Fig. 4a, which are at 45°. Knowing these

cooling angles will allow two components of velocity to be measured.

It is also important to ensure that the wires are insensitive to changes in pitch angle (α) induced by the unmeasured third velocity component. In an initial study of the regular single-component NSTAP probe, Vallikivi and Smits (2014) found that the pitch angle had little impact (<1 %) on the accuracy of the velocity measurement for a pitch angle range of $-20° \leq \alpha \leq 20°$. Figure 6 presents the wire velocity sensitivity for a single inclined NSTAP (with the sensing element angled at 45°, Fig. 4a) and a regular single-component NSTAP, as pitch angle changes while keeping the yaw angle of both probes to be at 0°, facing the incoming flow. The regular NSTAP is found to have a deviation due to the pitch angle of <2 % for $-15° \leq \alpha \leq 15°$,very similar to what was reported by Vallikivi and Smits (2014). Meanwhile, pitch angle has a much more dramatic impact on the single inclined wire NSTAP, with measurement inaccuracy exceeding 10 % for pitch angles greater than approximately 10°. The deviation of the inclined NSTAP is likely due to the asymmetric configuration of probe body which affects the flow field and the effective blockage.

Figure 7 shows the sensitivity to pitch angle for three different two-wire x-NSTAPs, with different wire spacings. For these sensors, the wire spacings (distances between the two probe bodies) are 50, 150, and 390 μm. The behavior for different pitch angles is very similar to what was observed for a single inclined NSTAP wire, but with an offset of each wire's minimum velocity reading. Since this offset from 0 pitch angle is only present in the two-wire x-NSTAPs measurements but not in the inclined single-wire NSTAP, it must be due to the supporting structure of one wire influencing the other wire. Therefore, unfortunately, the current x-NSTAP design is only suited to flows where the unmeasured component of velocity is known to be small and does not result in large wire pitch angles.

In order to improve the accuracy and decrease the sensitivity to pitch, the design of the probe body needs to be modified to reduce the influence on the flow. This is most effectively done by reducing the size of the probe support (currently in etched Silicon). We propose to do so by replacing the bulky silicon prongs with tungsten (W) tipped prongs which has the potential to reduce the size substantially and therefore decrease the aerodynamical effects observed in Fig. 6.

The novel technique to combine several MEMS devices presented above can be applied to combine more than two probes as well as other types of probes. For example, a regular NSTAP and a T-NSTAP (which will be explored in Sect. 2.3) can be combined to simultaneously measure the streamwise velocity and temperature fluctuations in a turbulent flow. Furthermore, we can add a third probe with another piece of patterned Kapton film, for example, an x-NSTAP and a T-NSTAP, to record two-component fluctuating velocities $\widetilde{u}$, $\widetilde{v}$, and the fluctuating temperature θ at the same time. This allows one to measure the wall-normal turbulent transport of temperature ($-\overline{v\theta}$). Such measurements are currently not possible and of great importance since they are an important component in wall-bounded turbulent heat-transfer problems.

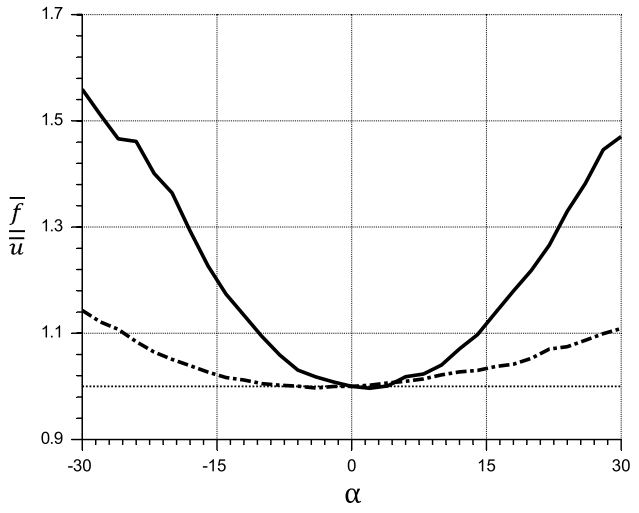

Fig. 6 A comparison of the velocity sensitivity between an inclined single-wire NSTAP angled at 45° (*solid curve*) and a regular NSTAP (*dashed curve*). It is clear that the regular NSTAP gives quite accurate measurements especially when the pitch angle α is small, while the inclined NSTAP is affected much more from the pitch angle. This is taken at free stream velocity of $\overline{u} = 14$ m/s. Note that the inclined NSTAP has the sensing element at 45° to the incoming flow at $\beta = 0$

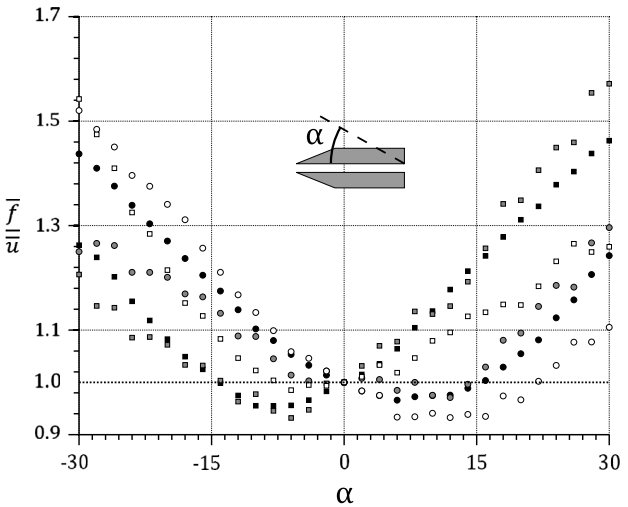

Fig. 7 x-NSTAP wire velocity sensitivity as it varies with pitch angle for three cases: x-NSTAPs with wire spacing of 50 μm (*white*), 150 μm (*gray*), and 390 μm (*black*). *Circular* and *square symbols* represent each wire of an x-NSTAP. Free stream velocity is $\overline{u} = 14$ m/s

2.3 Temperature: T-NSTAP

Apart from velocity fluctuations, other flow parameters may be of interest too, such as the instantaneous temperature field. With the successful demonstration of the NSTAP for measuring instantaneous streamwise velocity, one would naturally consider using a similar process to improve the CW measurement technology. As opposed to HWA, where the wire is heated and therefore less sensitive to temperature, a CW utilizes an unheated wire that adapts to the flow temperature and results in a measurable change in wire resistance. Therefore, by measuring the CW resistance with a constant current circuit, one can determine the local temperature of the fluid.

In assessing the temperature responses of cold wires, Arwatz et al. (2013) recently developed a lumped parameter model for the dynamical behavior of CW and their supporting structure. Their study showed that end-conduction effects are more severe than previously thought and can lead to significant measurement errors. Since the model is developed based on the geometry and material properties of the sensors, it can also be used as a sensor design tool to optimize the response and minimize the end-conduction effects. An improved MEMS temperature sensor was developed guided by the CW model. The new sensor, named the T-NSTAP, was designed specifically for high-frequency temperature measurements. The performance of the T-NSTAP was evaluated in a heated grid-turbulence flow with constant mean temperature gradient (for more details about the setup, see Arwatz et al. 2015).

The T-NSTAP closely follows the design of a regular NSTAP with modifications based on the cold-wire model. According to the model, an improved performance can be achieved through a support structure that has higher thermal conductivity. Therefore, instead of a single platinum layer, a 200 nm layer of gold is deposited as the prongs because of its high thermal conductivity (more than four times of platinum). Low-frequency response was further improved by shortening the sensor support by 1 mm, which reduces the thermal mass of the probe and therefore reduces low-frequency attenuation. The length of the wire was increased to 200 μm, about three times of a regular NSTAP, yet more than one order of magnitude shorter than conventional cold wires. The rectangular cross section of the T-NSTAP wire filament is the same as the regular NSTAP, measuring 100 nm × 2 μm (Figs. 8, 9).

Of great interest in the study of scalar turbulence is the spectrum of temperature fluctuations, which is directly related to the variance of the temperature fluctuations. Figure 10 displays the temperature variance data obtained with a conventional CW and the T-NSTAP at different cross-stream locations in a heated grid turbulence with constant mean temperature gradient. As can be seen, the

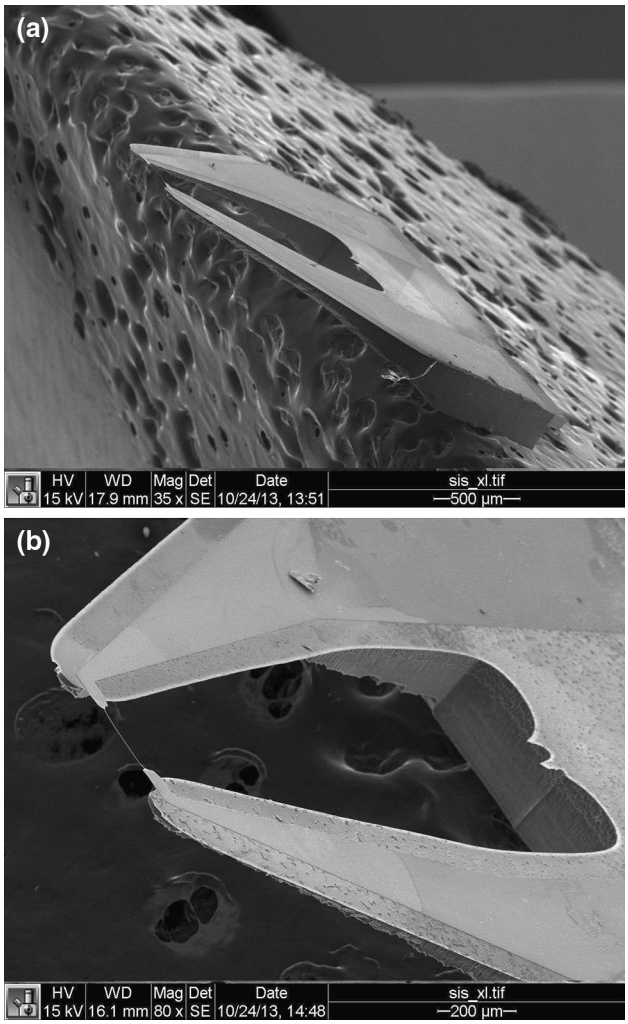

Fig. 8 SEM images of the T-NSTAP: **a** angular view of the probe showing metal side where Pt wire and two Au prongs resting on Si substrate. The aerodynamically shaped prongs are created by RIE-lag on Si. **b** A closer look at the free-standing Pt wire and Au prongs. The porous background is the conductive tape used for imaging

CW data are attenuated by approximately 25 % through all streamwise positions. Since the variance is the integral of the spectra, this important quantity is directly affected by the observed attenuation in the cold wire along with other quantities such as the integral scale.

The effect is even more drastic when investigating quantities related to the dissipation spectrum, namely

$$D_\theta(k) = 2\alpha k^2 F_\theta(k), \tag{2}$$

where F_θ is the one-dimensional temperature spectra, k is the wave number, and α is the thermal diffusivity. A close look at the peak of the dissipation spectra measured using a T-NSTAP and a cold wire (Fig. 11) reveals a significant attenuation of ~30 % as compared to the T-NSTAP. As in the case of the temperature spectra, the observed

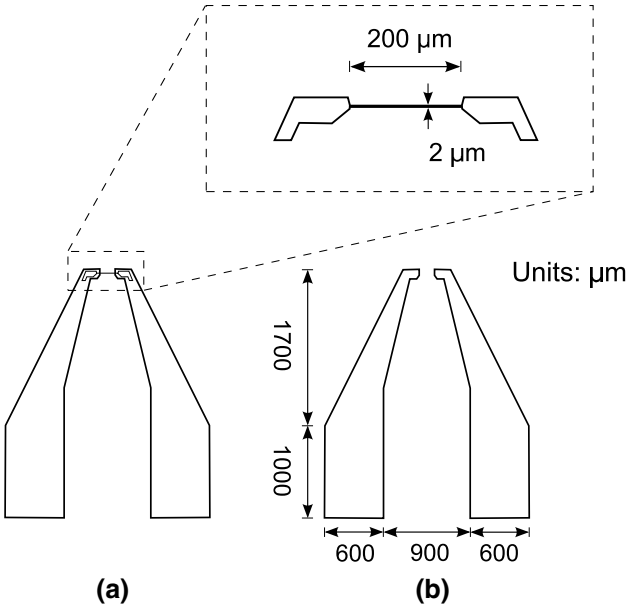

Fig. 9 T-NSTAP two-layer metal design: **a** metal side of the probe includes the Pt wire (more details in the *dashed rectangle*) and Au prongs. **b** Shape and dimension of the Au prongs. Figure excerpted from Arwatz et al. (2015)

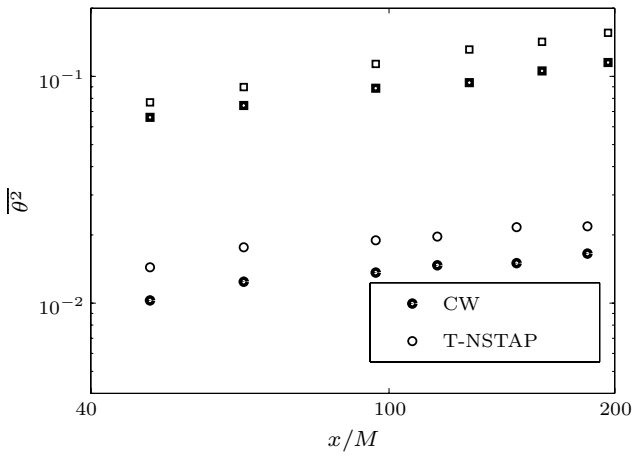

Fig. 10 Temperature variance for a cold wire and a T-NSTAP for $\overline{u} = 6$ m/s (*lower curves*, *circle symbol*) and $\overline{u} = 9$ m/s (*higher curves*, *square symbol*). *x* / *M* represents different cross-stream locations in a heated grid-turbulence setup with a constant mean temperature gradient

attenuation has a significant effect on integrated quantities, specifically the scalar rate of dissipation,

$$\epsilon_\theta = \int_0^\infty D_\theta(k)\mathrm{d}k \tag{3}$$

Calculating ϵ_θ, an important parameter for scalar turbulence, from the measurements presented in Fig. 11 reveals an attenuation of ~35 %. Applying the model developed in

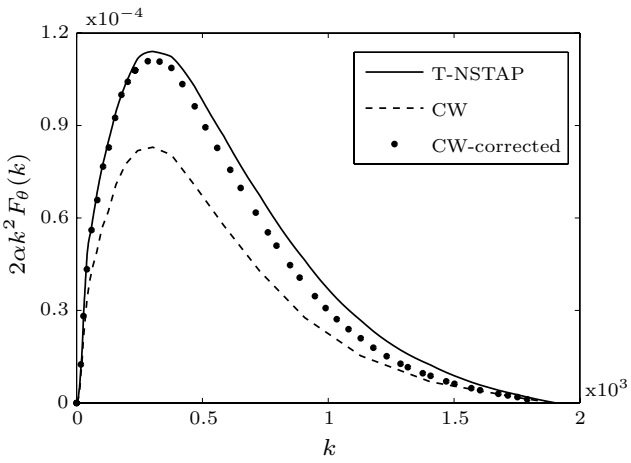

Fig. 11 One-dimensional temperature dissipation spectra measured using a cold wire and T-NSTAP. Figure excerpted from Arwatz et al. (2015)

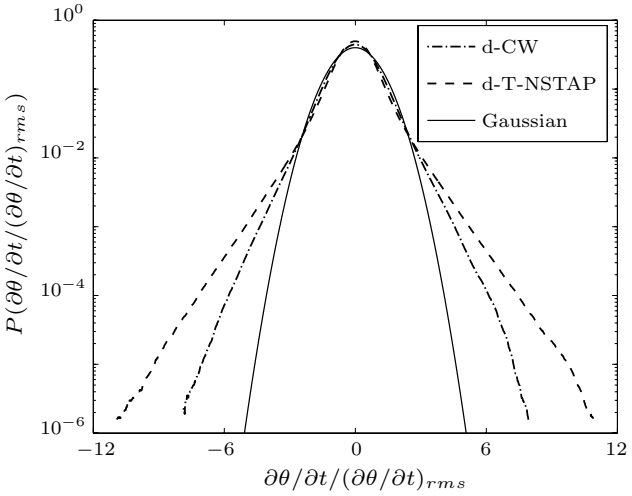

Fig. 12 PDF of the derivative $\partial\theta/\partial t$ measured using both a CW and a T-NSTAP. *Solid line* represents Gaussian distribution. Figure excerpted from Arwatz et al. (2015)

Arwatz et al. (2013) to the cold-wire data of Fig. 11 results in a corrected scalar rate of dissipation within 4 % of the one obtained through the T-NSTAP measurements.

Furthermore, the probability density functions (PDFs) of the temperature fluctuations and their derivatives also reveal a significant difference between the T-NSTAP and the conventional CW. As predicted and observed by previous studies (Pumir et al. 1991; Jayesh and Warhaft 1991, 1992), the PDF exhibits exponential tails in the presence of a mean scalar gradient, associated with high amplitude rare events. Figure 12 shows an example of the PDF of the derivative $\partial\theta/\partial t$ for both sensors. Even wider tails are observed in the T-NSTAP data, probably a result of rare events with short timescale being filtered by a conventional cold wire.

2.4 Humidity: q-NSTAP

The most recent addition to the NSTAP family is a fast-response humidity sensor, the q-NSTAP. As first noted by Bailey et al. (2010), when the NSTAP sensing element decreases in size, its sensitivity to velocity also decreases. This phenomenon was explained as the effect of low Péclet number (*Pe*) for heat transfer. The Péclet number is defined as the ratio between the heat transport by convection and by conduction:

$$Pe = \frac{l_c u_c}{\alpha} = RePr, \tag{4}$$

where l_c is the characteristic length, u_c is the characteristic velocity (in this case, $u_c = \overline{u}$, the mean streamwise velocity), and α is the thermal diffusivity. The Péclet number can also be expressed as the product of the Reynolds number *Re* and the Prandtl number *Pr*. When the local Péclet number of the hot wire is less than unity, the molecular diffusion dominates the heat transport over convection and therefore becomes less sensitive to flow velocity. Despite an undesirable effect while measuring velocity, it can be utilized to measure the humidity, since the thermal conductivity of air is known to be a function of humidity (see, e.g., Tsilingiris 2008; Beirão et al. 2012).

The humidity level in the air influences the thermal conductivity and thus affects the diffusion of heat. By measuring the heat transfer from the wire to the surrounding fluid in a similar fashion as a hot wire, one can isolate the humidity level as long as the Péclet number is small. Obtaining data with high spatial and temporal resolution of humidity fluctuation is very important for understanding the energy balance in the atmospheric boundary layer, as the humidity contributes to a substantial amount of energy being transported from the ground to the air in form of latent heat. Current humidity sensors are slow, large, and expensive, resulting in filtering and errors in the estimates of the latent heat transport.

The q-NSTAP wires need to be much smaller than regular NSTAPs in order to decrease their sensitivity to velocity. Therefore, a few additional modifications were implemented in the probe design and manufacturing. All the other probes in the NSTAP family are patterned with photolithography tools, which has a minimum feature size of around 800 nm depending on the type of light source (usually much higher). In order to deposit sensing wires that are even smaller, electron-beam (e-beam) lithography was used to write patterns that are about 500 nm in width. E-beam lithography uses high-energy electrons as the source, and combined with electron-sensitive resist, one can fabricate features as small as a few nanometers. Due to the reduced width of the wires, the length of the wire was also shortened to 10 μm to improve the structural rigidity of the sensing element. After depositing platinum as the sensing wire, the final width of the wires is typically between 600 and 800 nm. At such a small scale, even the internal stress from a thin film could damage the wires. To avoid that, an important procedure is to reduce the stress of the insulating thin film deposited between the bare silicon wafer and the platinum wires (see Vallikivi and Smits 2014 for more details). This is achieved by depositing alternating layers of silicon dioxide SiO_2 and silicon nitride SiN_x as insulating film, instead of a single layer of silicon dioxide as used for the other NSTAP sensors. This allows the internal stresses from SiO_2 and SiN_x to cancel each other out. With this method, the internal stress of the insulating layer was successfully lowered from about 450 to 40 MPa, and the structural integrity of the sensor substantially improved.

Due to the non-uniformity in lithography and metalization during the manufacturing processes, each probe will be slightly different in terms of sensing element dimension and, thus, its resistance. This requires the q-NSTAP probes to be individually calibrated before use. Since the thermal conductivity of air is a function of both temperature and humidity, it is crucial to know the exact wire temperature, in order to extract information about humidity. Therefore, the first step of calibration is to heat the wire to a few known temperatures around the operating temperature (usually 100–400 °C), record its resistance change and find the resistance–temperature characteristics. The actual operating temperature can then be extrapolated by measuring the wire resistance with the relationship $R_T = R_{\text{ref}}[1 + \gamma(T - T_{\text{ref}})]$,where R_T and R_{ref} correspond to the measured resistance and the reference resistance; T_{ref} is the temperature of which R_{ref} is recorded at; T is the temperature of interest and γ is the temperature coefficient of resistivity, which can be determined from the resistance–temperature characteristics plot. The q-NSTAP is then calibrated at a known velocity and operating temperature with different humidity levels. Even though the q-NSTAP will be operated in a regime where diffusion dominates, it is important to note that even if the Péclet number is less than unity, the effects from convection should not be entirely neglected. Therefore, when acquiring measurements, another velocity sensor, such as a regular NSTAP, should be deployed along with the q-NSTAP to simultaneously record flow velocity which can be used to correct the humidity data.

Due to the extremely low currents required operating the q-NSTAP (<1 mA), a modified circuit is also necessary. A custom-built constant-temperature anemometer (CTA) was developed, as described in Sect. 3 and has shown encouraging results during preliminary operation with frequency response around 0.5 MHz using a square-wave test. At this stage, the fabrication process along with the design is being optimized to further reduce the size of the sensor and then detailed measurements will follow.

3 CTA circuitry development for probe operation

The collection of NSTAP sensors is unique in size, resistance, and operating current compared to conventional sensors. Therefore, it was necessary to develop a custom CTA to conduct measurements (hereby called the PUCTA, Princeton University Constant-Temperature Anemometer). NSTAP wires are incredibly small by design, and depending on the size of the wire, electrical currents as low as 1 mA can destroy them. Also, the resistance of these wires is relatively high compared to common hot-wire probes (100–200 Ω NSTAP vs. 5–10 Ω tungsten wire at ~5 μm in diameter). These properties present difficulties when trying to operate on commercially available anemometers.

The CTA typically use some variation of the Wheatstone bridge as the feedback system (more information on Wheatstone bridge operation can be found at Ekelof 2001). Figure 13 presents a simplified schematic of a Wheatstone bridge for constant-temperature HWA. The ratio of the bridge resistance to the unheated wire resistance (commonly referred to as the "over-heat ratio") dictates the temperature of the wire when the circuit is stable. When a heated wire is placed in a flow field, it alters the temperature of the wire through convection, and this change in resistance is compensated by modifying the voltage into the bridge. This bridge voltage can be correlated to the flow velocity in a hot wire, or the water content in the q-NSTAP, for accurate and high bandwidth fluid measurement.

As the NSTAPs are being further miniaturized, they fail to operate with commercially available anemometers. This is due to the fact that these anemometers are designed for relatively large-sized wires [with resistance of $\mathcal{O}(10)\Omega$]. Normally, the top-of-bridge resistors (R_1 and R_2) are on the same order of the wire resistance for a one-to-one bridge. So for miniature wires such as the NSTAP [with $R_{\text{wire}} = \mathcal{O}(100)\,\Omega$], even though the amount of current is reduced due to a higher total resistance, the current limit that the wire can take is also lowered because of a much thinner wire. This will result in quick heating up of the NSTAP to be over its oxidation temperature and therefore "burns" the wire. There are two ways to solve this: reducing the voltage range that can enter the circuit (which reduces overall measurement accuracy) and simply by increasing the resistance of R_1.

The increased resistance of the NSTAP also impacts the stability characteristics of the system. The regular NSTAPs (with $90\ \Omega \leq R_{\text{wire}} \leq 150\,\Omega$) have had marginal success in stability with conventional anemometers (the Dantec Streamline CTA system in particular), but the ability to adjust the stability is lost. Wires with lower- or higher-resistance wires have been found to be unstable, which results in immediate wire breakage. Because of its higher resistance, a larger percentage of voltage drop will occur

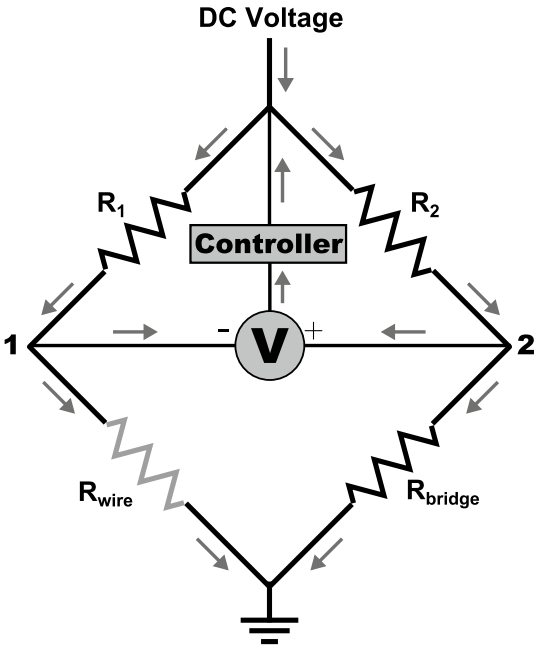

Fig. 13 Simplified schematic of a typical constant-temperature anemometry Wheatstone bridge configuration

across the NSTAP. This adds an unwanted variable gain into the feedback loop of the system, which inherently alters the stability characteristics. This could be solved in a number of ways, but to increase the resistance of R_1 is one of the easier approaches. It is important to note that there are many aspects of the circuit that impact the stability of the system including gain and filter values or even the inductance of the cable connecting the wire to the anemometer.

In both instances (too much current and inherent instability), the problem can be solved by changing the top-of-bridge resistors. What makes the PUCTA unique to commercially available anemometers is that all of the resistors within the bridge (R_1, R_2, and R_{bridge}) can be actively adjusted. This makes it easy to control the maximum current that can pass through the bridge as well as allows the users to scale the rest of the bridge resistors with the wire resistance for increased stability. With this relatively simple change, NSTAPs and q-NSTAPs can be operated with more adjustment flexibility, improved stability, and less wire failures compared to any commercially available unit.

So far, the PUCTA has had great success running NSTAPs, x-NSTAPs, and q-NSTAPs, all completely stable. For example, a typical velocity/voltage calibration of the x-NSTAP is shown in Fig. 14. As the velocity increases, the bridge voltage decreases to compensate for the wire's changing temperature. This indicates that the anemometer is working sufficiently for mean velocity measurements. To test the frequency response of the wire, it is common to

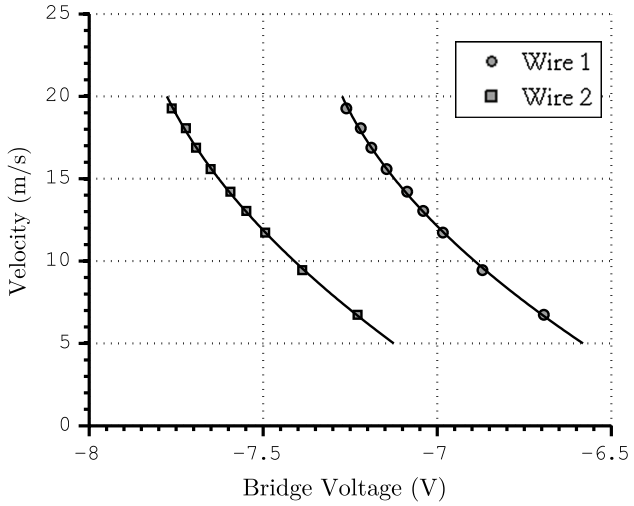

Fig. 14 Sample velocity/voltage calibration of the PUCTA anemometer using an x-NSTAP probe with two crossed wires

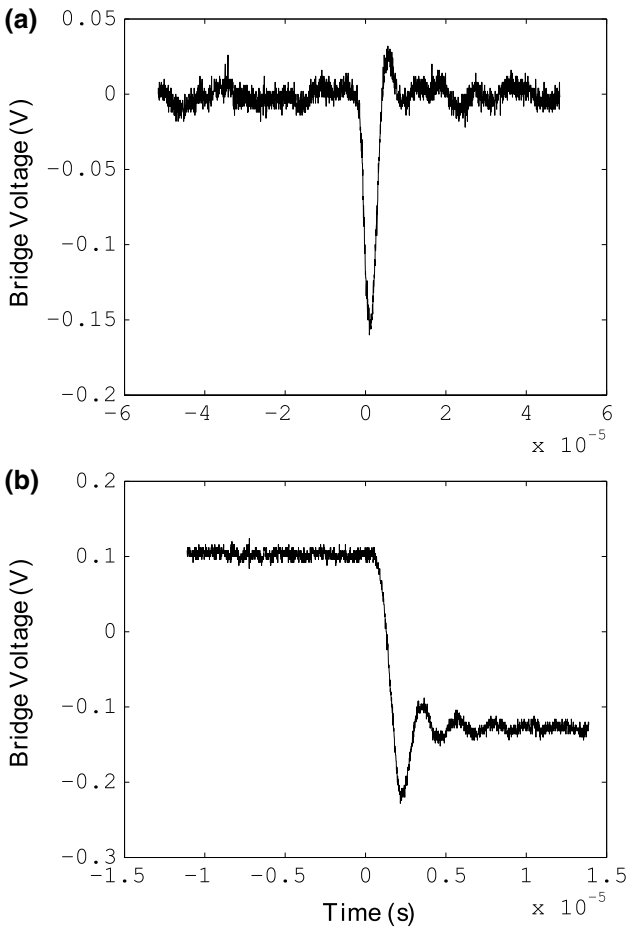

Fig. 15 Typical frequency responses for the regular NSTAP (**a**) and q-NSTAP (**b**) corresponding to responses of approximately 100 and 450 kHz, respectively. Note that for the q-NSTAP, (**b**) the DC of the square-wave input is not removed

analyze the response of the wire to a square-wave-induced impulse (even though it may not exactly reflect the "true" frequency response of the sensor as Hutchins et al. (2015) pointed out). Figure 15 displays a typical square-wave response of an NSTAP and q-NSTAP. Note here that for the NSTAP the DC component of the square wave is removed with a high-pass filter, and for the q-NSTAP, it is not (due to the anemometer going through some modifications during testing). As the bridge experiences a step in the voltage, the wire quickly adapts to the new configuration. The resulting frequency responses of the wires are 100 and 450 kHz for the NSTAP and q-NSTAP, respectively. These numbers are by no means universal, as it depends on the wire size, temperature, and flow conditions. However, they do indicate that the PUCTA circuit is capable of stabilizing the wire operation at extremely high frequencies.

Much work is still ongoing with the PUCTA. The circuit is being tested against commercially available anemometers to compare frequency response, electronic noise, anemometer sensitivity to temperature, and voltage drift, among other things. Also, a theoretical and experimental stability analysis is being conducted on the anemometer (much like the analysis conducted by Watmuff (1994) on the custom MUCTA anemometer). This will provide insight into the ideal anemometer settings for each type of NSTAP wire, maximizing measurement performance.

4 Conclusion

Measuring turbulence at high Reynolds number requires sensors with high spatial and temporal resolution. Here, we described a collection of nanoscale sensors specifically designed to measure two components of velocity, temperature, and humidity fluctuations with unprecedented resolution both temporally and spatially. The single-component NSTAP, T-NSTAP, and x-NSTAP have more than one order of magnitude higher spatial and temporal resolution compared to the conventional hot-wire, cold-wire, and cross-wire probes, respectively. Experimental studies with NSTAPs and T-NSTAPs have brought new insights into turbulence, previously masked by sensor filtering. A novel technique of combing multiple probes is presented, allowing compact packaging of multiple sensing elements. The x-NSTAP is manufactured by combining two single-wire NSTAPs with inclined wire filaments and is the first two-component MEMS velocity sensor designed for turbulence measurement. It is shown that the current design is sensitive to pitch of the sensor, which implies that it is only suitable where relative flow angles are low. These findings help guide the design of the next iteration of x-NSTAPs which will have even smaller probe supports. The novel method

of combining sensors allows construction of sensors that can measure different quantities simultaneously and effectively in the same location, which previously has not been possible. Finally, a novel approach to measure instantaneous humidity levels in turbulent flows is introduced. The humidity sensor, q-NSTAP, will enable fully resolved latent heat flux measurements in the lower atmosphere.

Acknowledgments The authors would like to thank Prof. Lex Smits for making all of the above-described sensors possible by pioneering MEMS-based turbulence measurements and for his many helpful comments and suggestions. This work was made possible through ONR grants N00014-12-1-0875 and N00014-12-1-0962 (program manager Ki-Han Kim) and the Fondation pour l'Etude des Eaux du Léman (FEEL). The development of the T-NSTAP and the q-NSTAP is part of the international, interdisciplinary research project elemo (http://www.elemo.ch) whose objective is to study and preserve freshwater resources.

References

Arwatz G, Bahri C, Smits AJ, Hultmark M (2013) Dynamic calibration and modeling of a cold wire for temperature measurement. Meas Sci Technol 24(12):125301

Arwatz G, Fan Y, Bahri C, Hultmark M (2015) Development and characterization of a nano-scale temperature sensor (t-nstap) for turbulent temperature measurements. Meas Sci Technol 26(3):035103

Ashok A, Bailey S, Hultmark M, Smits A (2012) Hot-wire spatial resolution effects in measurements of grid-generated turbulence. Exp Fluids 53(6):1713–1722

Bailey SC, Kunkel GJ, Hultmark M, Vallikivi M, Hill JP, Meyer KA, Tsay C, Arnold CB, Smits AJ (2010) Turbulence measurements using a nanoscale thermal anemometry probe. J Fluid Mech 663:160–179

Beirão S, Ribeiro A, Lourenço M, Santos F, de Castro CN (2012) Thermal conductivity of humid air. Int J Thermophys 33(8–9):1686–1703

Bodenschatz E, Bewley G, Nobach H, Sinhuber M, Xu H (2014) Variable density turbulence tunnel facility. Rev Sci Instrum 85(9):093908–093918. doi:10.1063/1.4896138

Borisenkov Y, Kholmyansky M, Krylov S, Liberzon A, Tsinober A (2015) Multiarray micromachined probe for turbulence measurements assembled of suspended hot-film sensors. J Microelectromech Syst PP(99):1. doi:10.1109/JMEMS.2015.2417213

Bradshaw P (1971) An introduction to turbulence and its measurement. Pergamon international library of science, technology, engineering, and social studies. Pergamon Press. ISBN 9780080166216

Brocard Y, Desplas P (1984) Vortical flow exploration methods developed for the f1 wind tunnel. In: In AGARD Wind Tunnels and Testing Tech. 15 p (SEE N84–23564 14–01), vol 1

Chen J, Fan Z, Zou J, Engel J, Liu C (2003) Two-dimensional micromachined flow sensor array for fluid mechanics studies. J Aerosp Eng 16(2):85–97

Ebefors T, Kalvesten E, Stemme G (1998) Three dimensional silicon triple-hot-wire anemometer based on polyimide joints. In: Micro electro mechanical systems, 1998. MEMS 98. Proceedings., the eleventh annual international workshop on, IEEE, pp 93–98

Ekelof S (2001) The genesis of the wheatstone bridge. Eng Sci Educ J 10(1):37–40

Ho C, Li W, Garstenauer M, Karan K, Leu T, Tai Y (1993) Micromachined hot-point anemometer. Part ii: testing and calibration. Bull Am Phys Soc 38:2234

Hultmark M, Ashok A, Smits AJ (2011) A new criterion for end-conduction effects in hot-wire anemometry. Meas Sci Technol 22(5):055401

Hultmark M, Vallikivi M, Bailey S, Smits A (2012) Turbulent pipe flow at extreme reynolds numbers. Phys Rev Lett 108(9):094501

Hultmark M, Vallikivi M, Bailey S, Smits A (2013) Logarithmic scaling of turbulence in smooth-and rough-wall pipe flow. J Fluid Mech 728:376–395

Hutchins N, Nickels TB, Marusic I, Chong M (2009) Hot-wire spatial resolution issues in wall-bounded turbulence. J Fluid Mech 635:103–136

Hutchins N, Monty J, Hultmark M, Smits A (2015) A direct measure of the frequency response of hot-wire anemometers: temporal resolution issues in wall-bounded turbulence. Exp Fluids 56(1):1–18

Jayesh, Warhaft Z (1991) Probability distribution of a passive scalar in grid-generated turbulence. Phys Rev Lett 67:3503–3506. doi:10.1103/PhysRevLett.67.3503

Jayesh, Warhaft Z (1992) Probability distribution, conditional dissipation, and transport of passive temperature fluctuations in grid-generated turbulence. Phys Fluids A Fluid Dyn (1989–1993) 4(10):2292–2307. doi:10.1063/1.858469

Jiang F, Tai YC, Ho CM, Karan R, Garstenauer M (1994) Theoretical and experimental studies of micromachined hot-wire anemometers. In: Electron devices meeting,1994. IEDM'94. Technical Digest., International, IEEE, pp 139–142

Kim S, Nam T, Park S (2004) Measurement of flow direction and velocity using a micromachined flow sensor. Sens Actuators A Phys 114(2):312–318

Kunkel G, Arnold C, Smits A (2006) Development of nstap: nanoscale thermal anemometry probe. In: Proceedings of the 36th AIAA fluid dynamics conference

Laufer J (1954) The structure of turbulence in fully developed pipe flow. National committee for aeronautics

Ligrani P, Bradshaw P (1987) Spatial resolution and measurement of turbulence in the viscous sublayer using subminiature hot-wire probes. Exp Fluids 5(6):407–417

Löfdahl L, Stemme G, Johansson B (1989) A sensor based on silicon technology for turbulence measurements. J Phys E Sci Instrum 22(6):391

Löfdahl L, Stemme G, Johansson B (1992) Silicon based flow sensors for mean velocity and turbulence measurements. Exp Fluids 12:391–393

Marusic I, Monty JP, Hultmark M, Smits AJ (2013) On the logarithmic region in wall turbulence. J Fluid Mech 716:R3

Nickels T, Marusic I, Hafez S, Hutchins N, Chong M (2007) Some predictions of the attached eddy model for a high reynolds number boundary layer. Philos Trans R Soc A Math Phys Eng Sci 365(1852):807–822

Pumir A, Shraiman BI, Siggia ED (1991) Exponential tails and random advection. Phys Rev Lett 66:2984–2987. doi:10.1103/PhysRevLett.66.2984

Rosenberg B, Hultmark M, Vallikivi M, Bailey S, Smits A (2013) Turbulence spectra in smooth-and rough-wall pipe flow at extreme reynolds numbers. J Fluid Mech 731:46–63

Sinhuber M, Bodenschatz E, Bewley GP (2015) Decay of turbulence at high reynolds numbers. Phys Rev Lett 114(3):034,501

Smits A, Perry A, Hoffmann P (1978) The response to temperature fluctuations of a constant-current hot-wire anemometer. J Phys E Sci Instrum 11(9):909

Smits A, Monty J, Hultmark M, Bailey S, Hutchins N, Marusic I (2011) Spatial resolution correction for wall-bounded turbulence measurements. J Fluid Mech 676:41–53

Smits AJ, Hultmark M (2014) Nanoscale instrumentation for measuring turbulence. In: Proceedings of 19th Australasian Fluid Mechanics Conference (Melbourne, Australia, 8–11 Dec) 19:11–17

Tai Y, Jiang F, Liu C, Wu R, Ho C (1993) Micromachined hot-point anemometer. Part i: design and fabrication. Bull Am Phys Soc 38:2234

Talamelli A, Persiani F, Fransson JH, Alfredsson PH, Johansson AV, Nagib HM, Rüedi JD, Sreenivasan KR, Monkewitz PA (2009) Ciclopea response to the need for high reynolds number experiments. Fluid Dyn Res 41(2):021407

Townes HW, Gow J, Powe R, Weber N (1972) Turbulent flow in smooth and rough pipes. J Fluids Eng 94(2):353–361

Townsend AA (1976) The structure of turbulent shear flow, 2nd edn. Cambridge University Press, Cambridge

Tsilingiris P (2008) Thermophysical and transport properties of humid air at temperature range between 0 and 100 c. Energy Convers Manag 49(5):1098–1110

Vallikivi M, Smits A (2014) Fabrication and characterization of a novel nanoscale thermal anemometry probe. J Microelectromech Syst 23(4):899–907. doi:10.1109/JMEMS.2014.2299276

Vallikivi M, Hultmark M, Bailey S, Smits A (2011) Turbulence measurements in pipe flow using a nano-scale thermal anemometry probe. Exp Fluids 51(6):1521–1527

Vallikivi M, Hultmark M, Smits A (2012) Turbulence measurements at high reynolds numbers using a new inclined nano-scale thermal anemometry probe. In: Proceedings of 18th Australasian Fluid Mechanics Conference (Launceston, Australia, 3–7 Dec) 18:179–82

Wang YH, Lee CY, Chiang CM (2007) A mems-based air flow sensor with a free-standing micro-cantilever structure. Sensors 7(10):2389–2401

Watmuff JH (1994) A high-performance constant-temperature hot-wire anemometer. NASA Contractor Report 177645

Willmarth WW, Sharma LK (1984) Study of turbulent structure with hot wires smaller than the viscous length. J Fluid Mech 142:121–149

Wyngaard J (1968) Measurement of small-scale turbulence structure with hot wires. J Phys E Sci Instrum 1(11):1105

Zagarola MV, Smits AJ (1998) Mean-flow scaling of turbulent pipe flow. J Fluid Mech 373:33–79

Zhao R, Smits AJ (2007) Scaling of the wall-normal turbulence component in high-reynolds-number pipe flow. J Fluid Mech 576:457–473